 doi:10.20944/preprints202201.0247.v1

Communication

$Nd_2Fe_{14}B$/FeCo Core-Shell Nanoparticle Synthesis Using Galvanic Substitution Based Electroless Plating

Muhammad Aneeq Haq[1,2], Yoseb Song[2], HanSaem Lee[2], Mi Hye Lee[2], Bin Lee[2] and Bum Sung Kim[2,*]

[1] University of Science and Technology, 34113 Daejeon, Republic of Korea;
[2] Korea Institute of Industrial Technology, 21999 Incheon, Republic of Korea;
* Correspondence: bskim15@kitech.com;

Abstract: Core-shell structured magnetic nanoparticles combine hard and a soft phases to improve energy efficiency. The mutual interaction of the two phases can lead to the exchange spring effect leading to higher magnetic energy. In this regard, synthesis of $Nd_2Fe_{14}B$ based core-shell structured powders have proven to be elusive due to the relatively reactive nature of this phase. In this study, a process has been established for successfully coating the surface of $Nd_2Fe_{14}B$ powders with FeCo layer using galvanic displacement method. Initially, a binary phase magnetic powder was synthesized containing $Nd_2Fe_{14}B$ and Nd_2Fe_{17} phase. Subsequently, the powders were coated using a Co precursor at 303 K. During coating the metastable Nd_2Fe_{17} phase was dissolved and the Fe ions were released into the solution. Subsequently, the Fe ions deposited together with the Co ions on the surface of $Nd_2Fe_{14}B$ powder to form a FeCo shell. The deposited layer thickness and composition was confirmed using TEM analysis.

Keywords: $Nd_2Fe_{14}B$; FeCo; Core-shell structure; galvanic substitution; Electroless plating

1. Introduction

Core-shell structured powders are a special class of materials having multifunctional properties [1–6]. This unique powder structure allows a convenient superimposition of the core and shell phase properties [5, 6]. Owing to their high functionality, core-shell structured powders have been developed for a wide range of applications including magnets [7–11], semiconductors [12], organic/inorganic composites [13, 14], and metal matrix composites [5, 15]. These specialized materials have allowed the researchers to go beyond the property limits of traditional single phase materials [5]. In particular, core-shell structured magnetic nanoparticles have the potential to achieve enhanced magnetic energy product [8]. This enhancement effect, known as the exchange-spring magnetic effect, is caused by the mutual interaction of hard and soft magnetic phase [16]. Exchange-spring effect has been successfully demonstrated on several hard magnetic systems including Nd-Fe-B [7], Sm-Co [8], Fe-Pt [10] and various ferrites [11]. These researches give ample evidence for the immense potential of spring magnets as highly energy efficient materials.

Theoretically, the $Nd_2Fe_{14}B$ based magnets are the most suitable material system for obtaining spring magnets. Atomistic studies and finite element simulations have revealed the superior potential of the $Nd_2Fe_{14}B$ based core-shell powders in realizing the maximum magnetic energy [17, 18]. However, given the complexity of the $Nd_2Fe_{14}B$ crystal structure, the fabrication of such powder with a uniform soft magnetic coating is challenging. Therefore, despite the encouraging results in other magnetic systems, no such successful attempt obtaining core-shell structured $Nd_2Fe_{14}B$ powder has been reported. In this regard, there is an imminent need for developing a coating technique for obtaining an $Nd_2Fe_{14}B$ powder coated with a soft magnetic shell.

To that end, here we report the development of a novel process for synthesizing $Nd_2Fe_{14}B$ powder coated with a FeCo layer. Initially a nanostructured $Nd_2Fe_{14}B$ powder containing a metastable Nd_2Fe_{17} phase was fabricated by electrospinning, calcination and

 doi:10.20944/preprints202201.0247.v1

reduction of Nd, Fe and B precursors. Afterwards the electroless plating of the prepared powder was done in a Cobalt (Co) bath. During the plating process, the galvanic substitution of the metastable Nd_2Fe_{17} phase was done to ionize the Fe ions while preserving the $Nd_2Fe_{14}B$ phase. Concomitantly, the Fe ions were co-deposited along with Co on the surface of $Nd_2Fe_{14}B$. Finally, the formation of the FeCo layer was confirmed.

2. Materials and Methods

The starting $Nd_2Fe_{14}B$ powder was synthesized via electrospinning, calcination, reduction and washing process. Initially fibers were obtained by electrospinning of a PVP solution containing Nd, Fe and B precursors in an electrospinning machine (NSLAB, Elmarco). The resultant fibers were calcined in air to obtain Nd-Fe-B oxide fibers and remove the PVP. Afterwards the oxide fibers were reduced in an argon atmosphere using Calcium (Ca) granules at 1123 K. Finally, the reduced fibers were broken down into powder during washing. The detailed description of each step can be found elsewhere [19].

As a pretreatment before the FeCo coating, the hard magnetic powder was cleansed in methanol followed by the surface sensitization and activation treatments. Tin chloride dihydrate ($SnCl_2{\cdot}2H_2O$, 98%, Sigma-Aldrich Inc., USA) and palladium chloride ($PdCl_2$, 99%, Sigma-Aldrich) were used for the sensitization and activation treatment respectively. Finally, the powder was electroplated in a cobalt bath for obtaining a FeCo coating. The composition of the electroless plating solution was 0.09 M cobalt sulfate heptahydrate ($CoSO_4{\cdot}7H_2O$, 99%, Sigma-Aldrich Inc., USA), 0.25 M sodium hypophosphite monohydrate ($NaH_2PO_2{\cdot}H_2O$, Alfa Aesar Co., UK), 0.3 M sodium citrate dihydrate ($Na_3C_6H_5O_7{\cdot}2H_2O$, 99%, Thermo-Fisher Inc., USA), and 0.1 M diammonium sulfate ($(NH_4)2SO_4$, 99%, Sigma-Aldrich Inc., USA). The plating process was performed at a temperature of 303 K for 10 minutes, and the pH was kept at 9 using an aqueous solution of sodium hydroxide (NaOH, 93%, Duksan Co., Korea) having a concentration of 2 M.

The phase change, microstructure and composition of the powders were analyzed using X-ray diffraction analyzer (XRD), scanning electron microscope (SEM), energy dispersive X-ray spectroscopy (EDS), and transmission electron microscope (TEM). The shell formation mechanism was analyzed through primary particle analysis. The average particle size and deviation were calculated by analyzing 50 particles using the ImageJ program.

3. Results

The morphological changes during each step of $Nd_2Fe_{14}B$ powder synthesis are shown in Fig. 1. After the electrospinning step, the obtained polymeric fiber had a smooth surface with a diameter of around 750 ± 50 nm (Fig. 1 (a)). Upon calcination, the diameter of the fibers reduced to 550 ± 100 nm as the water and organic constituents were removed (Fig. 1(b)). A high degree of porosity is visible in the calcined oxide fibers. The polymer to precursor ratio used for electrospinning was kept high to induce porosity within the fibers after calcination [20]. As a result, these fibers can be easily converted into nanosized powder during the subsequent processing. Figure 1 (c) shows the fiber morphology after reduction treatment in the presence of Ca granules. The Ca reacts with the oxide fibers and deposits on the fiber surface and within the pores in the form of CaO. The diameter at this stage increased to 900 ± 200 nm. Finally, the reduced sample was washed in an NH_4Cl solution to remove the CaO from the sample. The fibrous structure broke down during the washing step and nanosized powder was obtained. Fig. 1 (d) shows the resultant powders obtained by using ultrasonication of the washed sample. The finally obtained powder had an average particle size of 252 ± 38 nm. However, the nanosized powder particles were present in the form of agglomerates. Table 1 shows the fiber shape diameter information and the particle size analysis results of the nanocomposite powder.

Preprints (www.preprints.org) | NOT PEER-REVIEWED | Posted: 17 January 2022 doi:10.20944/preprints202201.0247.v1

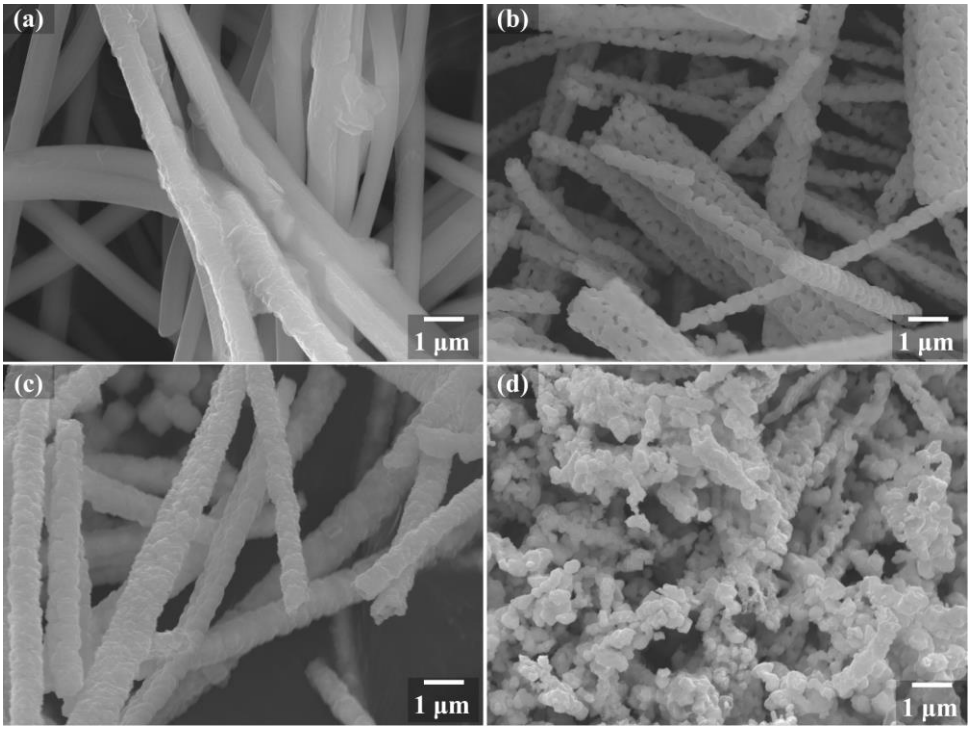

Figure 1. Micrographs of $Nd_2Fe_{14}B$ nanoparticle fabrication process after each stage; (a) as spun, (b) calcined, (c) reduced and (d) washed.

Process	As spun	Calcined	Reduced	Washed	Pre-treated	Deposited
Fiber diameter (nm)	750	550	900	-	-	-
Particle diameter (nm)	-	-	-	252	249	254
Distribution (±nm)	50	100	200	39	32	47

Table 1. Measured diameters of the sample at each process stage

The powder obtained after washing and ultrasonication was pretreated in Sn and Pd solutions for sensitization and activation respectively. This treatment is necessary for enhancing the deposition rate by activating the powder surface [21]. Figure 2 (a) shows the SEM and EDS mapping of the pretreated powder. The powder size and morphology of the pretreated powder remained similar to the as synthesized powder. The powder size was measured to be around 249 ± 32 nm. The EDS maps in Fig. 2(a) show a relatively uniform distribution of Pd while some evidence of unreacted Sn can be observed. This can be caused by inherent agglomeration of the nanosized powder which provides pockets for unreacted Sn deposition [8].

After the pretreatment, the resultant powders were treated in Co bath for obtaining FeCo coating on the powder surface. After 10 minutes of plating, the process was stopped and the powders were filtered, rinsed and dried. The Fig. 2 (b) shows the SEM and EDS mapping of the powder after electroless plating step. The size of the coated powder was measured to be 254±47 nm. However, the difference in size between pre-coated and coated powder was statistically insignificant. The EDS analysis confirmed a uniformly distributed presence of Co on the powder surface. This confirmed the successful plating of Co

Preprints (www.preprints.org) | NOT PEER-REVIEWED | Posted: 17 January 2022 doi:10.20944/preprints202201.0247.v1

on to the powder surface. Further analysis using XRD was done to confirm the phase changes.

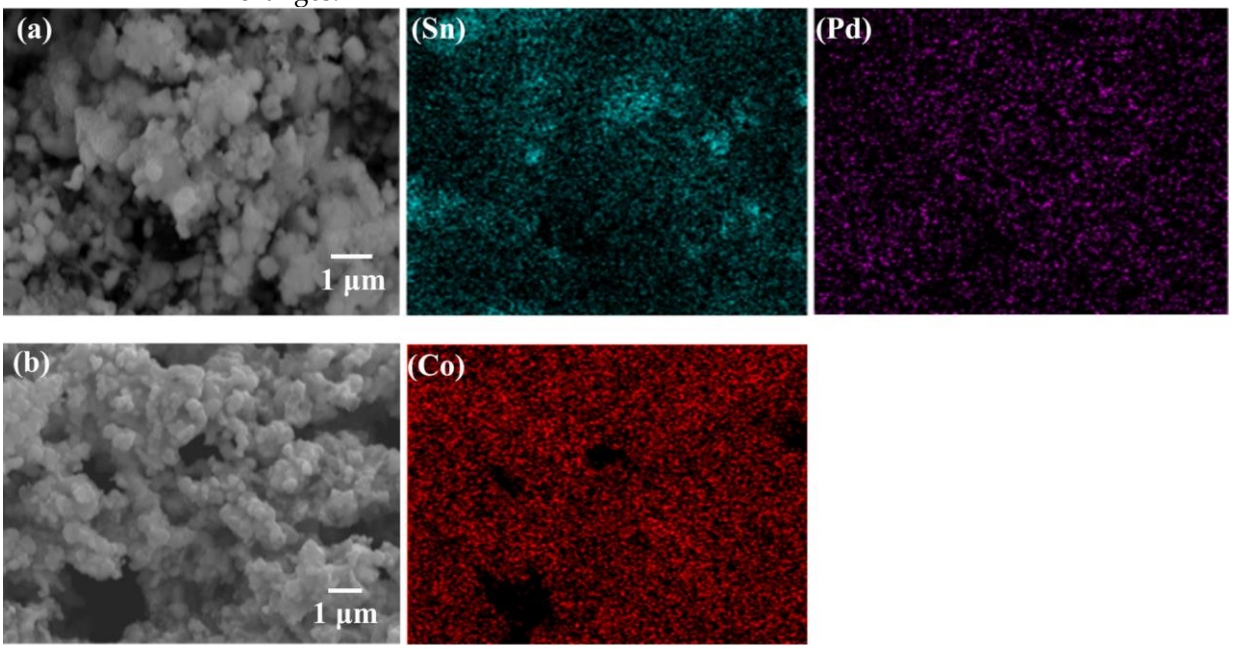

Figure 2. (a) SEM along with EDS mapping images of pre-treated Nd-Fe-B powder; (b) SEM along with EDS mapping images of the Co deposited powder.

The XRD analysis of the washed, pretreated and plated sample was carried out to confirm the phase composition of the powder. The XRD patterns are shown in Fig. 3. The XRD pattern of the as-prepared powder consisted of a main $Nd_2Fe_{14}B$ phase along with secondary phases of Nd_2Fe_{17} and α-Fe. The presence of secondary phase is inherent within the adapted synthesis procedure. After the calcination step, the fiber is made up of a Fe_2O_3, $FeNdO_3$ and $NdBO_3$ composite [22]. During the reduction, the composite oxide reduce together to form $Nd_2Fe_{14}B$. However, by reducing the boron content within the oxide fibers, the presence of Nd_2Fe_{17} and α-Fe phases can be induced.

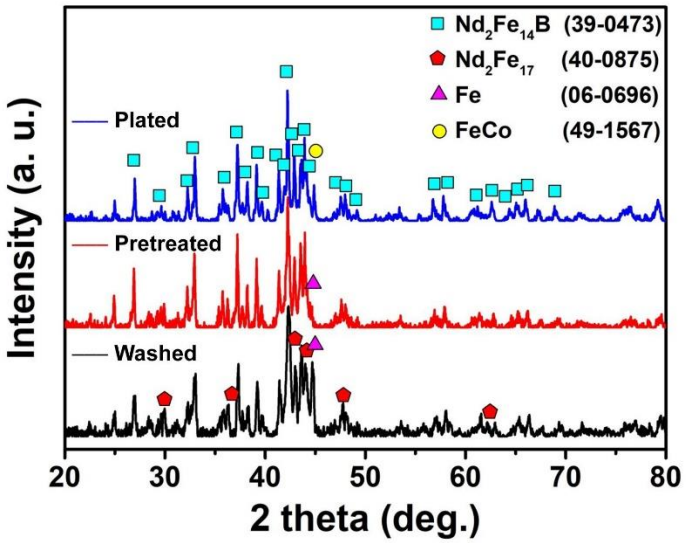

Figure 3. XRD patterns of the washed (black), Pre-treated (red) and plated (blue) samples.

The primary α-Fe phase peak can be clearly be seen at the 44.7°. The presence of Nd_2Fe_{17} peaks is however difficult to establish visually due to the presence of strong overlap with the $Nd_2Fe_{14}B$ peaks. In the XRD pattern of the sensitized and activated powder,

Preprints (www.preprints.org) | NOT PEER-REVIEWED | Posted: 17 January 2022 doi:10.20944/preprints202201.0247.v1

the α-Fe peaks were greatly reduced. The low pH of 1-2 used during pretreatment caused the dissolution of excess α-Fe while only $Nd_2Fe_{14}B$ and Nd_2Fe_{17} peaks remain. Finally, in the XRD patterns obtained after plating shows a reappearance of peak at 44.7°. This peak is presumed to be of the deposited FeCo phase as no separate Co peaks were observed alongside. The quantitative analysis of the FeCo plated XRD pattern confirmed a greatly diminished Nd_2Fe_{17} content in the final powder.

As the FeCo phase and α-Fe have a similar XRD pattern, it is difficult to distinguish between the two to confirm the composition of the coated phase. The TEM analysis of the powder surface was conducted to further verify the elemental composition and observe the layer thickness. Figure 4 shows TEM image superimposed with an EDX line map of electroless plated $Nd_2Fe_{14}B$ powder.

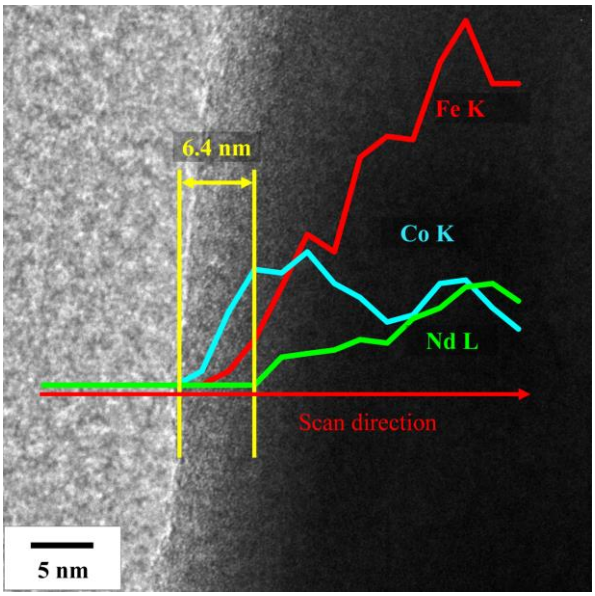

Figure 4. TEM image along with EDX line map taken from surface of the plated powder.

A thin layer of under 10 nm thickness can be observed at the powder surface. There is a clear interface present between the core and the shell phase. The EDX line map confirmed the presence of Fe and Co within the shell. In core region, the Nd and Fe concentrations become dominant. This confirms the formation of a core-shell structure formation between hard and soft magnetic phases. The thickness of the soft phase is sufficiently thin for developing exchange spring magnetic effect [16].

The formation of FeCo layer as well as the preservation of the $Nd_2Fe_{14}B$ phase confirms that the galvanic substitution progressed at the expense of Nd_2Fe_{17} during the plating process. The reported results confirm the possibility of obtaining soft phase coating on $Nd_2Fe_{14}B$ permanent magnetic powder by careful design of the reaction process. Based on these promising initial results, additional fine tuning will be carried out to attain a powder with ideal exchange spring magnetic effect. The content of the metastable phase needs to be adjusted to increase the Fe concentration within the shell phase. Additionally, the agglomeration of the nanosized powder needs to be controlled for obtaining a thorough coating of the shell phase around each individual $Nd_2Fe_{14}B$ particle.

4. Conclusions

Electroless plating of a soft magnetic FeCo phase on a hard magnetic $Nd_2Fe_{14}B$ nanoparticles has been successfully reported. The starting nanocomposite hard magnetic powder was synthesized using a modified electrospinning technique. The powder consisted of a primary $Nd_2Fe_{14}B$ phase along with a secondary phase of metastable Nd_2Fe_{17} phase. The starting powder surface was then subjected to sensitization and activation treatment followed by electroless plating in a Co bath. During the electroless plating, the Nd_2Fe_{17} phase preferentially ionized leaving behind only $Nd_2Fe_{14}B$ powder. Consequently, the ionized Fe from the Nd_2Fe_{17} phase co-deposited along with Co on to the surface of $Nd_2Fe_{14}B$ powder to form a soft magnetic shell. The XRD and TEM analysis confirmed that the deposited shell was of FeCo phase while the core was of $Nd_2Fe_{14}B$ phase. The thickness of the shell was measured to be under 10 nm. The designed process opens up a vital avenue for developing $Nd_2Fe_{14}B$ based spring magnetic materials which can possess unmatched magnetic energy product. Further research needs to be conducted for tuning the structural and compositional features of the shell to obtain optimal magnetic properties.

Author Contributions: Conceptualization, H.L. and Y.S.; methodology, H.L.; validation, M.H.L and B.S.K.; formal analysis, H.L and Y.S.; investigation, H.L.; resources, K.T.P, B.S.K.; data curation, M.A.H.; writing—original draft preparation, M.A.H. and Y.S.; writing—review and editing, M.A.H and Y.S; visualization, M.A.H..; supervision, M.A.H.; project administration, Y.S.; funding acquisition, K-T.P and B.S.K. All authors have read and agreed to the published version of the manuscript.

Funding: This research received no external funding

Data Availability Statement: The data supporting reported results can be requested from the corresponding author (B.S.K).

Conflicts of Interest: The authors declare no conflict of interest. The funders had no role in the design of the study; in the collection, analyses, or interpretation of data; in the writing of the manuscript, or in the decision to publish the results.

References

1. Ghosh Chaudhuri, R.; Paria, S. Core/Shell Nanoparticles: Classes, Properties, Synthesis Mechanisms, Characterization, and Applications. *Chem. Rev.* **2012**, *112*, 2373–2433, doi:10.1021/cr100449n.

2. B. Gawande, M.; Goswami, A.; Asefa, T.; Guo, H.; V. Biradar, A.; Peng, D.-L.; Zboril, R.; S. Varma, R. Core–Shell Nanoparticles: Synthesis and Applications in Catalysis and Electrocatalysis. *Chemical Society Reviews* **2015**, *44*, 7540–7590, doi:10.1039/C5CS00343A.

3. Min, Y.; Song, G.; Zhou, L.; Wang, X.; Liu, P.; Li, J. Silver@mesoporous Anatase TiO2 Core-Shell Nanoparticles and Their Application in Photocatalysis and SERS Sensing. *Coatings* **2022**, *12*, 64, doi:10.3390/coatings12010064.

4. Guo, W.; Zhang, H.; Zhao, S.; Ding, Z.; Liu, B.; Li, W.; Xu, H.; Liu, H. Corrosion Behavior of the CoNiCrAlY-Al2O3 Composite Coating Based on Core-Shell Structured Powder Design. *Materials* **2021**, *14*, 7093, doi:10.3390/ma14227093.

6. Ji, S.M.; Tiwari, A.P.; Kim, H.Y. Graphene Oxide Coated Zinc Oxide Core–Shell Nanofibers for Enhanced Photocatalytic Performance and Durability. *Coatings* **2020**, *10*, 1183, doi:10.3390/coatings10121183.

7. Li, H.; Li, X.; Guo, D.; Lou, L.; Li, W.; Zhang, X. Three-Dimensional Self-Assembly of Core/Shell-Like Nanostructures for High-Performance Nanocomposite Permanent Magnets. *Nano Lett.* **2016**, *16*, 5631–5638, doi:10.1021/acs.nanolett.6b02210.

8. Lee, J.; Kim, J.; Kim, D.; Lee, G.; Oh, Y.-B.; Hwang, T.-Y.; Lim, J.-H.; Cho, H.-B.; Kim, J.; Choa, Y.-H. Exchange-Coupling Interaction in Zero- and One-Dimensional Sm_2Co_{17}/FeCo Core–Shell Nanomagnets. *ACS Appl. Mater. Interfaces* **2019**, *11*, 26222–26227, doi:10.1021/acsami.9b02966.

9. Li, X.; Lou, L.; Song, W.; Huang, G.; Hou, F.; Zhang, Q.; Zhang, H.-T.; Xiao, J.; Wen, B.; Zhang, X. Novel Bimorphological Anisotropic Bulk Nanocomposite Materials with High Energy Products. *Advanced Materials* **2017**, *29*, 1606430, doi:10.1002/adma.201606430.

10. Zhang, W.; Yang, W.; Chandrasena, R.U.; Özdöl, V.B.; Ciston, J.; Kornecki, M.; Raju, S.; Brennan, R.; Gray, A.X.; Ren, S. The Effect of Core–Shell Engineering on the Energy Product of Magnetic Nanometals. *Chem. Commun.* **2018**, *54*, 11005–11008, doi:10.1039/C8CC05978K.

11. Dong, J.; Zhang, Y.; Zhang, X.; Liu, Q.; Wang, J. Improved Magnetic Properties of SrFe12O19/FeCo Core–Shell Nanofibers by Hard/Soft Magnetic Exchange–Coupling Effect. *Materials Letters* **2014**, *120*, 9–12, doi:10.1016/j.matlet.2014.01.022.

12. Reiss, P.; Protière, M.; Li, L. Core/Shell Semiconductor Nanocrystals. *Small* **2009**, *5*, 154–168, doi:10.1002/smll.200800841.

13. Naderi, N.; Sharifi-Sanjani, N.; Khayyat-Naderi, B.; Faridi-Majidi, R. Preparation of Organic–Inorganic Nanocomposites with Core-Shell Structure by Inorganic Powders. *Journal of Applied Polymer Science* **2006**, *99*, 2943–2950, doi:10.1002/app.22990.

14. Jia, H.; Quan, T.; Liu, X.; Bai, L.; Wang, J.; Boujioui, F.; Ye, R.; Vlad, A.; Lu, Y.; Gohy, J.-F. Core-Shell Nanostructured Organic Redox Polymer Cathodes with Superior Performance. *Nano Energy* **2019**, *64*, 103949, doi:10.1016/j.nanoen.2019.103949.

15. Haq, M.A.; Eom, N.S.A.; Su, N.; Lee, H.; Kim, T.S.; Kim, B.S. Powder Interface Modification for Synthesis of Core-Shell Structured CoCrFeNiTi High Entropy Alloy Composite. *Applied Surface Science* **2020**, *506*, 144925, doi:10.1016/j.apsusc.2019.144925.

16. Kneller, E.F.; Hawig, R. The Exchange-Spring Magnet: A New Material Principle for Permanent Magnets. *IEEE Transactions on Magnetics* **1991**, *27*, 3588–3560, doi:10.1109/20.102931.

17. Westmoreland, S.C.; Skelland, C.; Shoji, T.; Yano, M.; Kato, A.; Ito, M.; Hrkac, G.; Schrefl, T.; Evans, R.F.L.; Chantrell, R.W. Atomistic Simulations of α-Fe/Nd2Fe14B Magnetic Core/Shell Nanocomposites with Enhanced Energy Product for High Temperature Permanent Magnet Applications. *Journal of Applied Physics* **2020**, *127*, 133901, doi:10.1063/1.5126327.

18. Bance, S.; Oezelt, H.; Schrefl, T.; Winklhofer, M.; Hrkac, G.; Zimanyi, G.; Gutfleisch, O.; Evans, R.F.L.; Chantrell, R.W.; Shoji, T.; et al. High Energy Product in Battenberg Structured Magnets. *Appl. Phys. Lett.* **2014**, *105*, 192401, doi:10.1063/1.4897645.

19. Eom, N.S.A.; Jeon, E.J.; Haq, M.A.; Lee, J.; Choa, Y.-H.; Kim, B.S. Fabrication and Characterization of 1-Dimensional Neodymium-Iron-Boron Fibers Using New Reduction-Diffusion Process. *Materials Letters* **2020**, *268*, 127611, doi:10.1016/j.matlet.2020.127611.

20. Eom, N.S.A.; Noh, S.; Haq, M.A.; Kim, B.S. Synthesize of $Nd_2Fe_{14}B$ Powders from 1-D $Nd_2Fe_{14}B$ Wires using Electrospinning Process. *Journal of Korean Powder Metallurgy Institute* **2019**, *26*, 477–480, doi:10.4150/KPMI.2019.26.6.477.

21. Gulla, M.; Conlan, W.A. Catalyst Solution for Electroless Deposition of Metal on Substrate 1975.

22. Jeon, E.J.; Eom, N.S.A.; Choa, Y.-H.; Kim, B.S. Synthesis of One-Dimensional Neodymium-Iron-Boron-Oxides. *Materials Letters* **2020**, *264*, 127286, doi:10.1016/j.matlet.2019.127286.